

Article

# Methotrexate-Transferrin-Functionalized Fe(Salen)-Polypyrrole Nanocomposites for Targeted Photo-/Magneto-Thermal Cancer Treatments

Jeong-Hwan Kim <sup>1,2,\*</sup> , Masanari Umemura <sup>1</sup>, Haruki Eguchi <sup>3</sup> and Yoshihiro Ishikawa <sup>1</sup>

- <sup>1</sup> Cardiovascular Research Institute, Graduate School of Medicine, Yokohama City University, Yokohama 236-0004, Japan; umemurma@yokohama-cu.ac.jp (M.U.); yishikaw@med.yokohama-cu.ac.jp (Y.I.)  
<sup>2</sup> Bio-R&D Center, Fugenbio Co., Ltd., Seoul 06746, Korea  
<sup>3</sup> Technology Platform Center, Technology & Intelligence Integration, IHI Corporation, Yokohama 235-8501, Japan; eguchi1181@ihi-g.com  
\* Correspondence: jeongkim@yokohama-cu.ac.jp

**Abstract:** Designing multi-modal topical drug delivery nanocarriers using nano-hybrid particles has received significant interest in targeted cancer therapy. In this study, magnetic Fe(salen)-conducting copolymer nanocomposites based on our previous iron salt-free synthesis method are surface-functionalized with methotrexate and transferrin proteins. The nano-hybrids show near-infrared-/magnetic field-responsive hyperthermal activity *in vitro*, which can be extraordinarily useful in magnetically guidable local cancer targeting as a versatile multi-modal therapeutic drug delivery system.

**Keywords:** core-shell nanocomposites; photothermal; magneto-thermal; multimodal cancer targeting; targeted drug delivery



**Citation:** Kim, J.-H.; Umemura, M.; Eguchi, H.; Ishikawa, Y. Methotrexate-Transferrin-Functionalized Fe(Salen)-Polypyrrole Nanocomposites for Targeted Photo-/Magneto-Thermal Cancer Treatments. *J. Compos. Sci.* **2022**, *6*, 136. <https://doi.org/10.3390/jcs6050136>

Academic Editor: Konstantinos Tserpes

Received: 14 April 2022

Accepted: 5 May 2022

Published: 8 May 2022

**Publisher's Note:** MDPI stays neutral with regard to jurisdictional claims in published maps and institutional affiliations.



**Copyright:** © 2022 by the authors. Licensee MDPI, Basel, Switzerland. This article is an open access article distributed under the terms and conditions of the Creative Commons Attribution (CC BY) license (<https://creativecommons.org/licenses/by/4.0/>).

## 1. Introduction

Nanocarriers for topical drug delivery have emerged as powerful tools for non-invasive anticancer therapy with improved specificity and reduced side effects. Moreover, the combination of multiple therapeutic modalities, such as photo-thermal and magneto-thermal ablation, into a single nanocarrier has great potential to synergistically improve the efficacy of targeted anticancer therapies compared to monotherapy given individually [1–4]. However, each different modality possessed by such NPs should be fully maintained, rather than mutually compromising their original properties, resulting in, e.g., undesirable optical quenching, electron transfer blockage, or magnetic loss that is comprised of hysteresis loss and eddy current loss, due to the proximity of the individual components to the other materials. Surface functionalization permits us to make various reactive functional groups on the surface of NPs; to tether a variety of building blocks, such as NPs, ligands, biomolecules, drugs, and genes; and to build hybrid and multifunctional nanocomposites towards the evolution of drug delivery system (DDS) for multi-modal cancer diagnostics and therapeutics [3].

Most inorganic NP-based DDSs are still in their pre-clinical stage of progress. Among them, magnetic NPs (e.g., iron oxide nanoparticles (IONPs)) are one of the most commonly used NPs in biomedical field, as they have been reported as a non-invasive and highly effective agent for magnetic resonance (MR) contrast imaging and magneto-thermal ablation by numerous groups [2,3]. However, we have recognized that there are global problems related to the routine use of high-dose IONPs; the main problems associated with the use of IONPs in cell labeling/targeting include the digestion and removal of heavily-tagged cells from target tissues by macrophages and the perseverance of large residues of iron particles released from dying cells [5,6]. The iron is accumulated in the liver, spleen, and

thymus, inducing toxicity primarily in the liver and immune system, depending on the size and surface characteristics of the IONPs [7].

In order to address the issues of the utilization of IONPs by reducing the Fe dose and increasing the drug-loading capacity, we have recently demonstrated Fe(salen)-polypyrrole (PPy)-polycaprolactone (PCL)-core-shell nanoassemblies (referred to as CSNAs) [8] as a multifunctional anti-cancer agent, which showed four-fold capability in achieving magnetically guided drug delivery, magnetic resonance imaging (MRI), magnetic local hyperthermia, and chemotherapy. Unlike the existing IONP-based DDSs that require an additional binding process of drug reagents with IONPs, CSNAs utilize the intrinsic magnetism of molecular magnets (Fe(salen)) and their anticancer activity [9–13]. Maintaining multifunctionality in the simple molecular system with significantly reduced Fe content in response to magnetic fields and pH is extremely exclusive, and no similar systems have been reported.

Methotrexate (MTX) has been widely used as a major chemotherapeutic agent for human melanomas such as acute lymphoblastic leukemia, malignant lymphoma, osteosarcoma, breast cancer, and head and neck cancer [14]. Despite its efficacy, the intravenous administration of MTX is greatly limited due to its inability to reach the tumor site, leading to the damaging of normal tissues [14]. In order to deal with this problem, a wide range of the MTX-DDS have been studied, aiming to locate their cargo at the target tumors specifically [14–17].

Here, we propose to design nano-hybrid composites containing CSNAs and MTX prodrugs that can be utilized in local DDS for dual-modal targeted cancer therapy. An overview of the synthesis of the nano-hybrids of CSNAs with a conventional anticancer drug, MTX, is presented in Figure 1 (hereafter MTX-CSNAs). The tailor-made MTX-CSNAs were prepared by a unique covalent functionalization technique via cetylpyridinium (CPy) chemistry, which led to the complex nano-drug hybrids, integrating the attractive material properties into multi-functionalities such as photo-thermal (PT), magneto-thermal (MT), and chemotherapeutic efficacy.

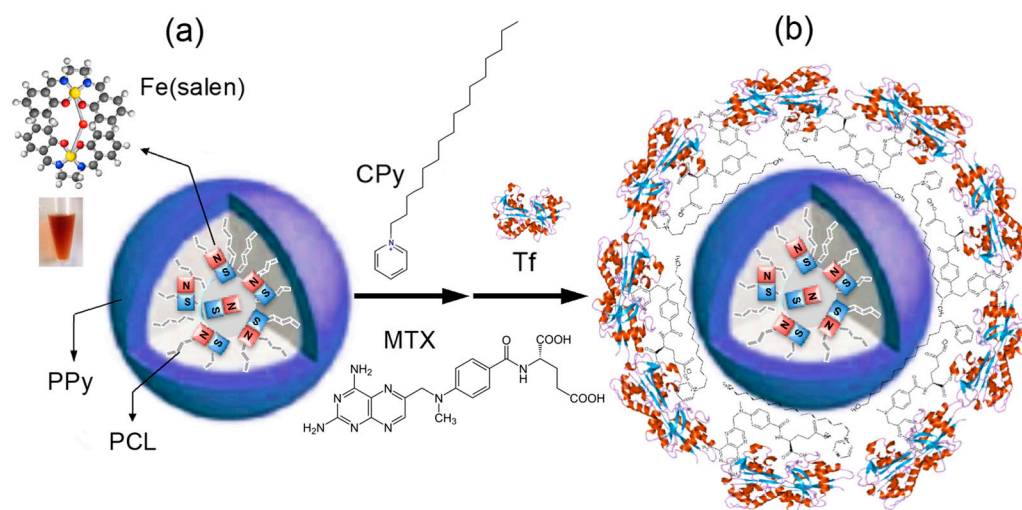


**Figure 1.** Synthesis of magnetic nano-hybrids functionalized with MTX and apo-transferrin (Tf) proteins as a surface stabilizer and cancer marker. (a) Fe(salen) molecules are loaded into PPy-*b*-PCL copolymers to form a core-shell nanoassembled NP. (b) MTX molecules are covalently functionalized onto the NP surface in the presence of CPy, followed by a colloidal stabilization via a transferrin coating.

The material characterization was performed using UV-vis spectroscopy, FT-IR spectroscopy, scanned transmission electron microscopy (STEM), electron spin resonance (ESR), cyclic voltammetry (CV), dynamic light scattering (DLS), and zeta potential analysis. The photodynamic and magneto-thermal responses were monitored with a confocal NIR-guided

PT measurement module in the threshold power range (0.1 W for NIR) and an alternating magnetic field (AMF)-induced MT measurement module, respectively. In this work, we aimed to study the NIR-PT-/AMF-MT-based DDS by employing the controlled assembly of the anticancer agent, MTX, and tumor specific marker, Tf molecules, on the dual modality-responsive CSNA NPs.

## 2. Experimental

### 2.1. Reagents

Iron salen was purchased from TCI. Other chemical reagents, including CPy chloride and apo-Tf powder samples, were purchased from Sigma-Aldrich (St. Louis, MO, USA) at high purity. MTX was purchased from Wako Pure Chemical Industries (Osaka, Japan). HeLa cell lines were obtained from the Japan Health Science Foundation, Health Science Research Resources Bank (Osaka, Japan).

### 2.2. Preparation of the Fe(Salen)-PPy Core–Shell Nanoassemblies (CSNAs)

CSNA samples were obtained according to the previous report [8]. Briefly, 10 mg Fe(salen) (Tokyo Chemical Industry Co., Ltd., Tokyo, Japan) in methanol solution was mixed with 2.5 mL 0.5 wt% PP solution (Sigma-Aldrich), and then briefly sonicated. After vigorous stirring for 15 min, the black CSNAs were precipitated and collected by a magnetic separation in order to ensure that it was free of unloaded Fe(salen) and PPs. Fe(salen) was incorporated into the PCL domain of PP by a hydrophobic interaction, rapidly formulating micelle-like CSNAs with a drug-loading capacity of approximately 90 wt%, as described in the previous report [8].

### 2.3. Preparation of Tf-MTX-Coated CSNAs and Tf-Coated CSNAs

Firstly, the black CSNA suspension in DIW (1.5 mg/mL) was mixed with 10 mg CPy Chloride by thorough sonication, and then adjusted to pH 8 with KOH. After reaction for 1 h, the sample was washed with alkaline water (pH 8) three times, by employing a magnetic separation. Subsequently, MTX (DMSO, pH 8, 2 mg/mL) was added into the CPy-CSNA sample, followed by a reaction for 1 h, which was then washed with saline (pH 8) three times by using a magnetic separation to remove unbound MTX molecules. The collected MTX-CSNA sample pellets were briefly sonicated and stored at 4 °C. The Tf-MTX-coated CSNAs or Tf-CSNAs were prepared by adding an excess amount of the apo-Tf sample (Sigma-Aldrich, 50 mg) into the CPy-CSNA or CSNA sample, respectively. The sample mixtures in saline were washed with sonication for ~10 s (pulsed mode), followed by an ultracentrifugation at 150,000 rpm for 30 min, and then washing steps with the support of magnetic separation three times in order to confirm the full removal of any unbound Tf molecules. The Tf-MTX-CSNA and Tf-CSNA sample pellets were briefly sonicated and stored at 4 °C.

### 2.4. Characterizations

The MTX-surface functionalization was determined using a Nanodrop UV-vis spectrophotometer (Fisher-Scientific, Pittsburgh, PA, USA). The FTIR spectra were recorded on a JASCO FT/IR-4100 spectrophotometer (JASCO, Tokyo, Japan) in transmission mode and in ATR mode. The particle structure was observed using a Gatan Titan TEM operating at 100–300 kV (FEI). The colloidal size distribution and stability were characterized by DLS and Zeta potential analysis, respectively, using a Malvern Nanosizer (Malvern, Herrenberg, Germany). In order to measure the magnetic intensity of the CSNA samples, electron spin resonance (ESR) analysis was conducted using a BioSpin ESR EMX-8/2.7 system (Bruker, Billerica, MA, USA), operating at a 9.9 GHz modulation frequency at room temperature. The microwave power and modulation amplitude were 1 mW and 1 G, respectively. The powder samples were prepared in a glass capillary sample holder and placed in a probe head (for four measurements per sample).

### 2.5. Cell Culture

HeLa cells were incubated in Dulbecco's modified Eagle's medium (DMEM) (Thermo, Waltham, MA, USA, SH30021.01), added with 10% fetal bovine serum (FBS) (Thermo, SH30910.03) and the antibiotics (10,000 mg/mL) streptomycin and 10,000 units per mL penicillin, at 37 °C in a humidified atmosphere containing 5% CO<sub>2</sub> (*v/v*). Sub-culturing was executed every three days, and 10<sup>6</sup> cells were seeded on a 10 cm Petri dish. The culture media were replenished with fresh media and cultured for a further 48 h. After dispensing 100 mL of cell suspension (5000 cells per well) in a 96-well plate, the plate was pre-incubated for 24 h in a humidified incubator.

### 2.6. Photo-Thermal Cancer Treatments

The plasmonic photo-thermal effect of the CSNA products was examined using a near infrared (NIR) diode laser system (IR-800) (custom-made by New Vision Inc., Taiwan, <http://www.nvi-laser.com/>, accessed on 9 March 2015) with a wavelength of 800 nm, as was similarly performed in the literature [18]. The laser diode was set 0.5 cm above the liquid surface and, upon the application of NIR-laser irradiation, 0.15–0.5 W laser power in continuous wave mode was used to irradiate the HeLa cells either in the absence or presence of JCNs in 10 mM PBS buffer. The heat sensing was performed with a thermocouple microprobe in a hyperthermia instrument, DM-100 (nB nano-Scale Biomagnetics, Zaragoza, Spain), submerged in the solution in a 1 cm<sup>2</sup> cuvette. The probe was located at such a position that the direct irradiation of the laser on the probe was evaded. After staining with a LIVE/DEAD Cytotoxicity Kit for mammalian cells (L-3224, Life Technologies, Carlsbad, CA, USA) for 5 min, microscopy images of the cells were obtained using a Zeiss LSM 510 multiphoton confocal microscope system through a 40× objective lens.

### 2.7. Magneto-Thermal Cancer Treatments

For the measurement of the magneto-thermal activity of the CSNAs, an AMF generator with a vertical coil, with an inner diameter of 4 cm, driven by a transistor inverter (Hot Shot, Ameritherm Inc., Scottsville, NY, USA) was used. The experiments were conducted at a frequency of 307–308 kHz and 378.8 A, unless otherwise specified [8]. A thermometer (hand-held thermometer HA-200, Anritsu Meter Co., Tokyo, Japan) or a thermograph (InfraRed camera, Nippon Avionics Co., Ltd., Tokyo, Japan) was used to determine the temperature *in vitro*.

### 2.8. Cell Viability Imaging and Assay

Following the photo-/magneto-thermal treatment, the cells were grown for 24 h. The viability of the cells was evaluated by counting live/dead cells with a TC20 automated cell counter (BioRad, Hercules, CA, USA). Following the cell staining according to the manufacturer's protocol (Cell Counting Kit-8, Dojindo, Tokyo, Japan), bright field/fluorescence imaging was carried out using an inverted Nikon Eclipse Ti confocal microscope (Melville, NY, USA). The cell viability assay was performed using the commercially available kit, a sodium 2,3-bis(2-methoxy-4-nitro-5-sulfophenyl)-5-[(phenylamino)-carbonyl]-2H-tetrazolium inner salt (XTT) assay cell proliferation kit (ATCC, Manassas, VA, USA). The cytotoxic effect by the NIR-/AMF-induced hyperthermia was monitored by confocal microscopy.

## 3. Results and Discussions

### 3.1. Preparation and Characterization of Tf-MTX-CSNAs

Fe(salen) molecules as a magnetic core were loaded into a PPy-*b*-PCL copolymer in order to form the CSNA structure, as described earlier [8]. The CSNAs show not only enhanced drug loading capacity because of each light-weighted component (compared with relatively heavy-weighted IONPs) but also increased magnetization properties due to the magnetic coupling between the Fe(salen) cores and PPy shells. Then, MTX drug

molecules were covalently conjugated on the CSNAs, using a CPy chloride linker in a manner similar to that in the literature [17].

As we previously studied, the PPy surface of CSNA is partially doped with *p*-toluenesulfonate (25%), which causes immediate aggregation in an aqueous solution due to the dominant hydrophobic interaction between the adjacent particles. In order to aid the desirable water-solubility, natural molecules such as gum arabic (GA) or bovine serum albumin (BSA) as the coating materials showed the successful surface functionality of the CSNAs, delivering high water-solubility and colloidal stability against heating and long-term storage [8]. This simple functionalization method may also offer the ease of the further conjugation of other drug (e.g., paclitaxel, doxorubicin, folic acid) or ligand (e.g., proteins, antibodies, aptamers, receptors) components. In this study, we employed transferrin (Tf) proteins for a direct surface stabilization via non-covalent adsorption, which does not require additional ligand conjugation steps unlike former ones, allowing us to specifically target cancer cells, where Tf-receptors are highly located in common tumour sites. In order to confirm the conjugation efficacy of MTX on the CSNA-CPy interface, we conducted UV-vis absorbance and FT-IR spectroscopy (Figure 2). The absorbance spectra of MTX-CSNAs (Figure 2a) showed a substantially enhanced emission curve in the 350–400 nm (TSPR region of MTX), compared to bare CSNAs, which confirmed the high-rate (~55%) conjugation of MTX molecules on the NPs. Besides this, the FT-IR spectrum of the MTX-CSNAs directly showed that MTX was present on the CSNA surface, as the IR spectrum exhibited characteristic peaks of MTX molecules (Figure 2b). The FT-IR spectra of the samples showed a broad band around  $3410\text{ cm}^{-1}$ , due to the OH stretching of water. After the MTX conjugation, the MTX characteristic absorption bands appeared at  $1025\text{ cm}^{-1}$ , which is due to the asymmetric and symmetric  $\text{CH}_3$  bending vibrations, and in the low-frequency region, the distinct presence of the band at  $1157\text{ cm}^{-1}$  is attributed to C=O vibration. A weak shoulder also appeared at  $1619\text{ cm}^{-1}$ , which could be assigned to the C=O and NH stretching, and all of these characteristics were confirmed to be similar to those of the MTX molecule [17]. Accordingly, the FT-IR spectra demonstrated that MTX had been conjugated onto the CPy of the PPy interfaces.

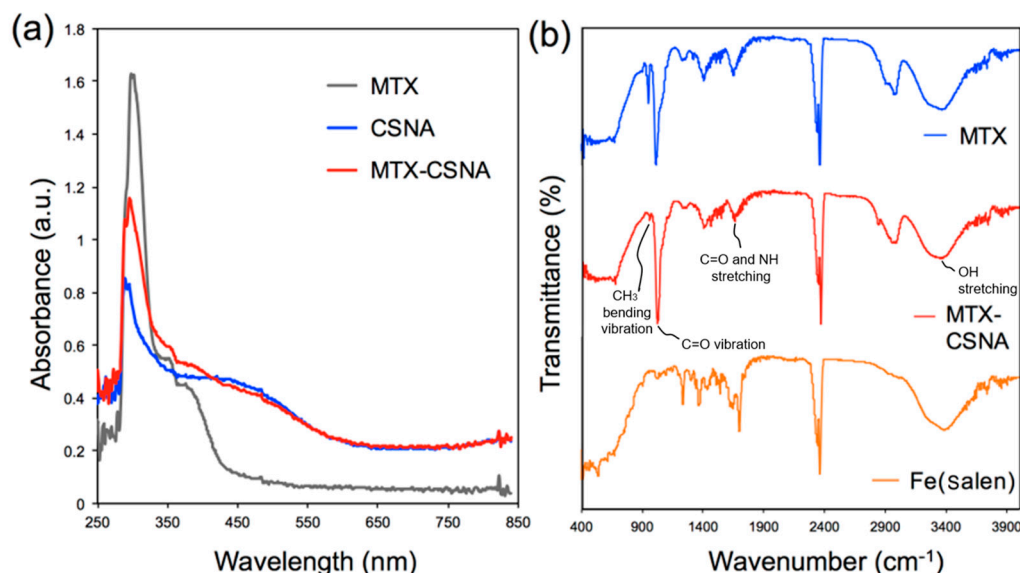


**Figure 2.** Optical characterization of MTX-CSNA NPs. (a) UV-vis absorbance and (b) FT-IR spectra, determining the successful conjugation of MTX drugs on the CSNA surface via CPy linkers.

The Cyclic voltammetry showed that the typical redox curve of Fe(salen) molecules at  $\sim 0.5\text{ V}$  disappeared in the CSNA sample, while showing typical redox PPy curves at nearly  $\pm 0.4\text{ V}$  [17], as shown in Figure 3. This confirms the successful surface encapsulation of Fe(salen) inside the matrix of PPy-*b*-PCL copolymers.

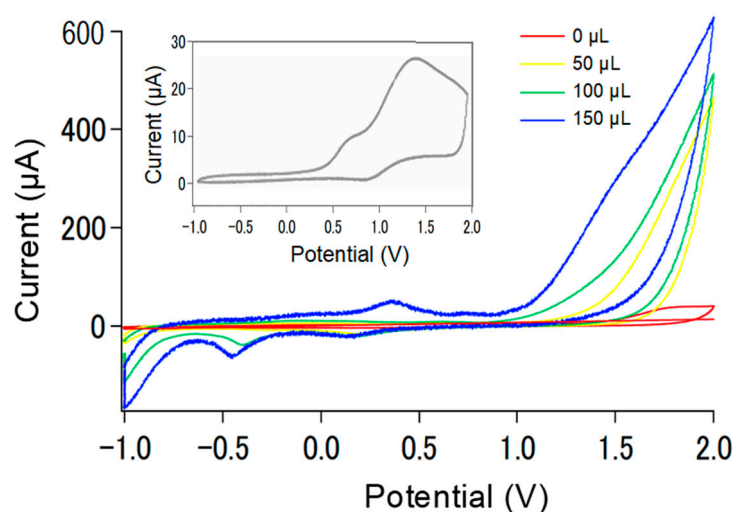


**Figure 3.** Cyclic voltammograms of Fe(salen)-PPy NPs in acetonitrile at 25 °C. Complex concentration: 0.001 M; supporting electrolyte: 0.1 M TBAP; scan rate: 100 mV/s; working electrode: Pt sphere; reference electrode: Ag/Ag<sup>+</sup>. The inset shows the CV of Fe(salen).

The structure of CSNA samples was characterized by STEM in order to verify the organic amorphous morphology, showing no magnetite formation inside the copolymer matrix, as we confirmed in the earlier study [8]. The low-magnification images of the CSNAs showed an aggregated form due to their hydrophobicity and multicore-shell morphology with ~45 nm size (Figure 4a). The brighter dispersed contrast within the CSNA matrix seems to be an entity of the Fe(salen) cores. However, the FFT of the enlarged profile confirmed that the NPs are fully amorphous without containing any substantial aggregates, which is in good agreement with the previous results [8]. This structure offers two principal advantages: (i) it maintains a fixed spatial configuration between the Fe(salen) cores inhibiting aggregation; and (ii) it provides an efficient platform for a strong magnetic coupling between the Fe cores upon assembly. Unfortunately, the structural imaging of MTX-CSNA and Tf-MTX-CSNA was challenged by the undesirable salt formation during the drying process in the TEM sample preparation. Instead, we performed dynamic light scattering (DLS) to determine the size of the samples, which revealed that the size distribution of Tf-MTX-CSNAs is 298.6 nm with good monodispersity (polydispersity index: 0.48) (Figure 4c), indicating that the conjugate complexes seem to be not solid but highly flexible in solution, which is consistent with the results of the BSA- or GA-functionalized samples [8]. The zeta potential value of the Tf-MTX-CSNA sample was  $-18$  mV, indicating its successful Tf surface passivation and relatively stable colloidal property when compared with the zeta potential value of polymer-passivated NPs in the literature [19] (Figure 4d).

In order to evaluate the magnetic behaviour of MTX-NPs over plain NPs, ESR measurements with the same mass of composite powder samples (5 mg) for both samples were performed (Figure 5). The magnetization curves of both samples at 300 K showed nearly identical intensities with typical ferromagnetic-like behavior [9], which indicates that the MTX-NPs retain their magnetic stability without losing any substantial magnetic characters for magnetically guidable drug delivery. Assuming that the Fe(salen) core composition is similar in both MTX-NPs and NPs, the CPy-assisted MTX-conjugation process on the NPs did not affect any alteration in either a morphological or magnetic fashion. The observed magnetic stability can be attributed to the close-packed surface functionalization of the CPy-MTX-Tf layer at the PPy interface over the NPs.

### 3.2. Biological Activities

The anticancer effect of the MTX-conjugated CSNAs was evaluated by XTT assay. As presented in Figure 6, the CSNAs did not show any cytotoxicity or effect on cell proliferation, as in the control. Instead, the MTX-micelles using CPH-based conjugation (MTX-CSNA

II) showed the most efficient anticancer cytotoxicity (<40%) in the concentration range of 30  $\mu\text{g}/\text{mL}$ , as compared with the other micelles (CSNA and the EDC-based MTX-micelle conjugates (MTX-CSNA I)), which confirms the successful linking of MTX on the PPy-shell of the CSNAs. The lack of toxicity of the CSNAs is presumed to protect the drug payload (Fe(salen)) from undesirable events (e.g., leakage) affecting the body, while the cytotoxic effect of MTX-linked CSNAs was achieved by the anticancer drug (MTX) binding well to the CSNA surface. On the other hand, the binding method by EDC (MTX-CSNA I) exhibited lower anticancer performance than the CSNA II, due to its relatively low binding efficiency.

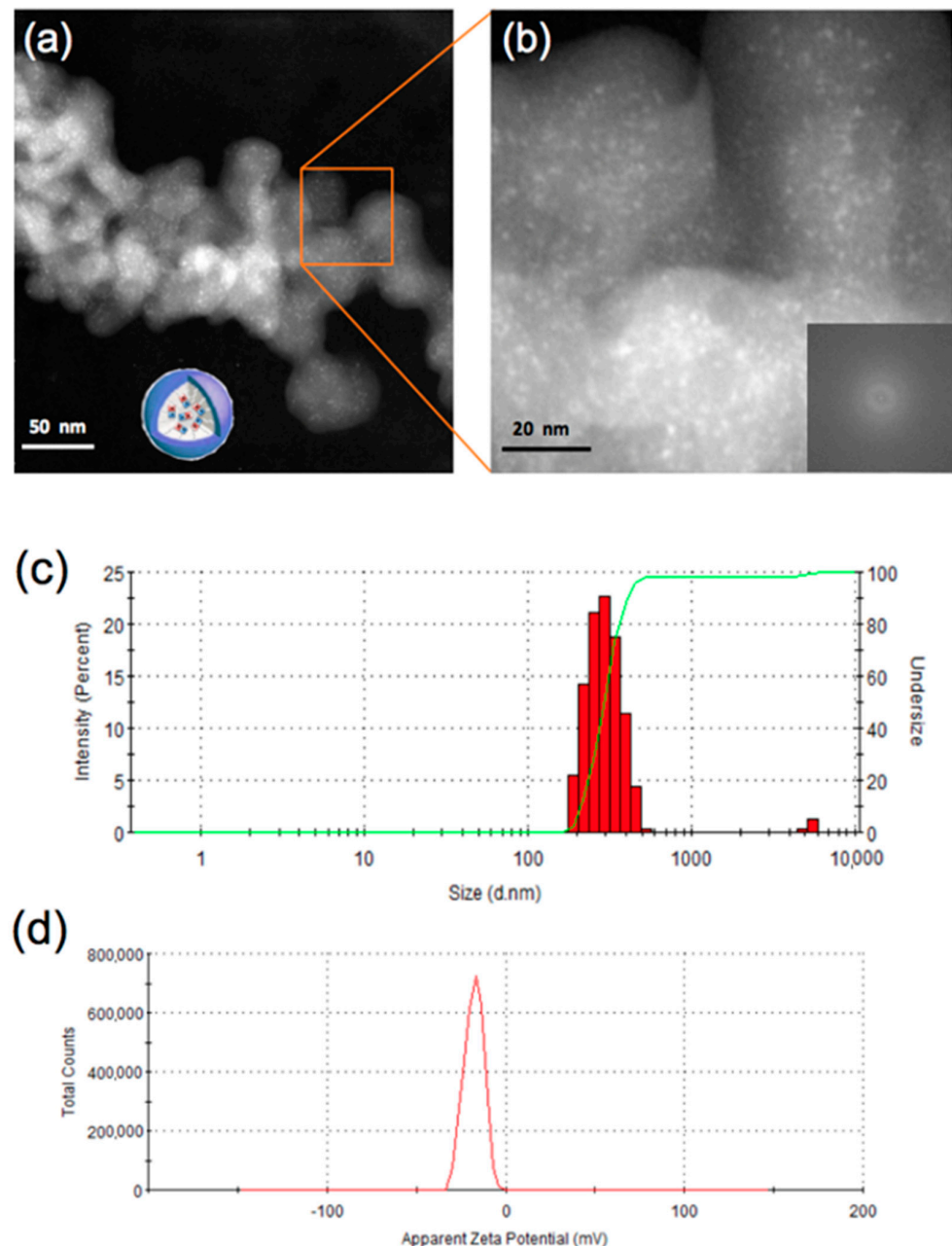


**Figure 4.** (a) Low-magnification STEM image of the as-prepared Tf-MTX-CSNAs. (b) The magnified STEM image of the NPs, showing their multicore-shell morphology. The FFT analysis (inset) shows that the NPs are amorphous, which confirms the organic basis of the NPs. (c) The DLS size distribution and (d) zeta potential analysis of Tf-MTX-CSNAs, exhibiting their good monodispersity and fair colloidal stability.

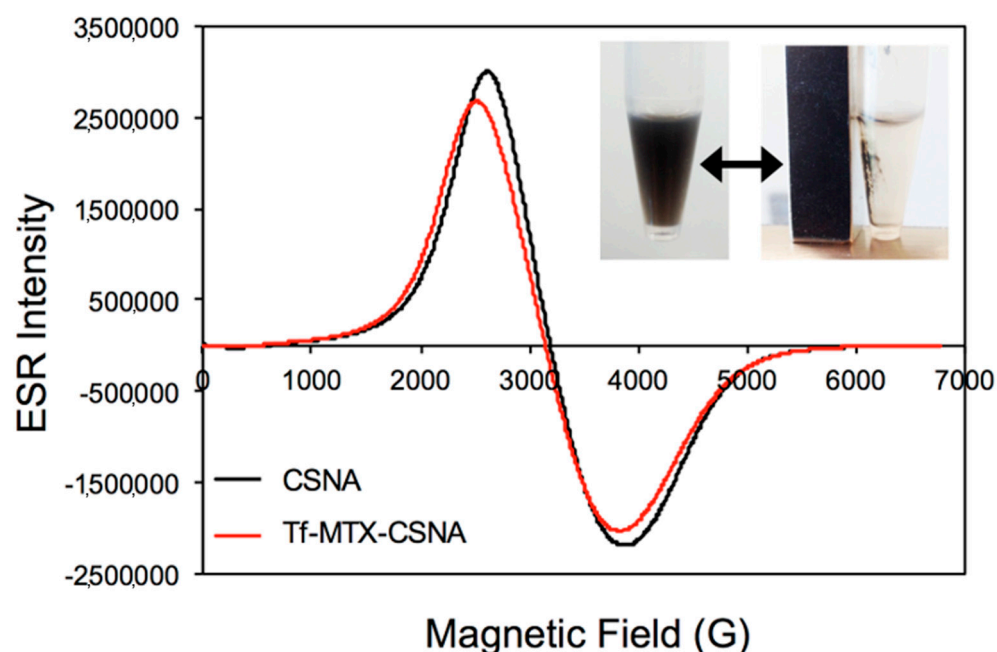


**Figure 5.** ESR-Magnetic characterization of CSNA and Tf-MTX-CSNAs, showing their outstanding ferromagnetic behavior without the loss of stability. The inset shows how the Tf-MTX-CSNAs can be magnetically guided and/or concentrated using a commercially available conventional magnet.

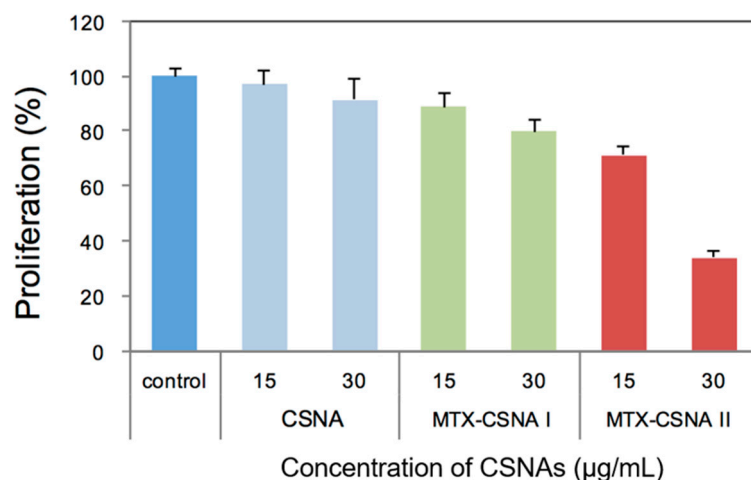


**Figure 6.** Cytotoxicity evaluation of MTX-CSNAs. XTT assay of CSNA, MTX-CSNA I (EDC/NHS coupling-based), and MTX-CSNA II (CPy-based). MTX-CSNA II showed substantial cytotoxicity over the other samples, reflecting the fact that the MTX molecules are well-coated onto CSNAs via the CPy-based functionalization method.

### 3.3. Dual-Modal Hyperthermia Activities

The CSNA NPs showed plasmon adsorption in the near-infrared region of the electromagnetic spectrum (650–800 nm), which likely may endow photo-thermal effects. In the present work, an experimental setup was established in order to evaluate the photo-thermal properties of these NPs when irradiated by NIR. The temperature of the suspension of NPs (Figure 7) increases by  $\sim 7^\circ\text{C}$  after 1 min of irradiation with continuous-wave 800 nm laser light at 0.1 W. The enhanced efficiency of the photon-to-heat conversion exhibited by the NP suspension can be attributed to PPy encapsulation on the NPs. In fact, heat conduction in a nanostructured PPy shell is usually dominated by phonons even for PPy which has metal-like properties, and which is expected to have an important contribution from electron heat transfer [20,21]. Photo-thermal nanocomposites are materials that combine

nano-thermodynamic and nano-optical properties, and their main function of interest is to control the heat generation of nanoparticles through light absorption [20,21]. Although metal NPs are known as a common example of thermoplasmonics as an efficient heating source at the surface plasmon resonance (SPR) frequency, other types of photo-thermal nanomaterials apart from metals, such as conjugated polymers, have been also studied [22]. Among the various conductive polymers, PPy is a potential photo-thermal material as a light-absorbing polymer with a high electrical conductivity when doped with other suitable dopants [20,21]. Although research has been focused on the thermoelectric properties of pure PPy or PPy composites [21], it has never been studied at the level of nanocomposite particles with bimodal properties as in this study.

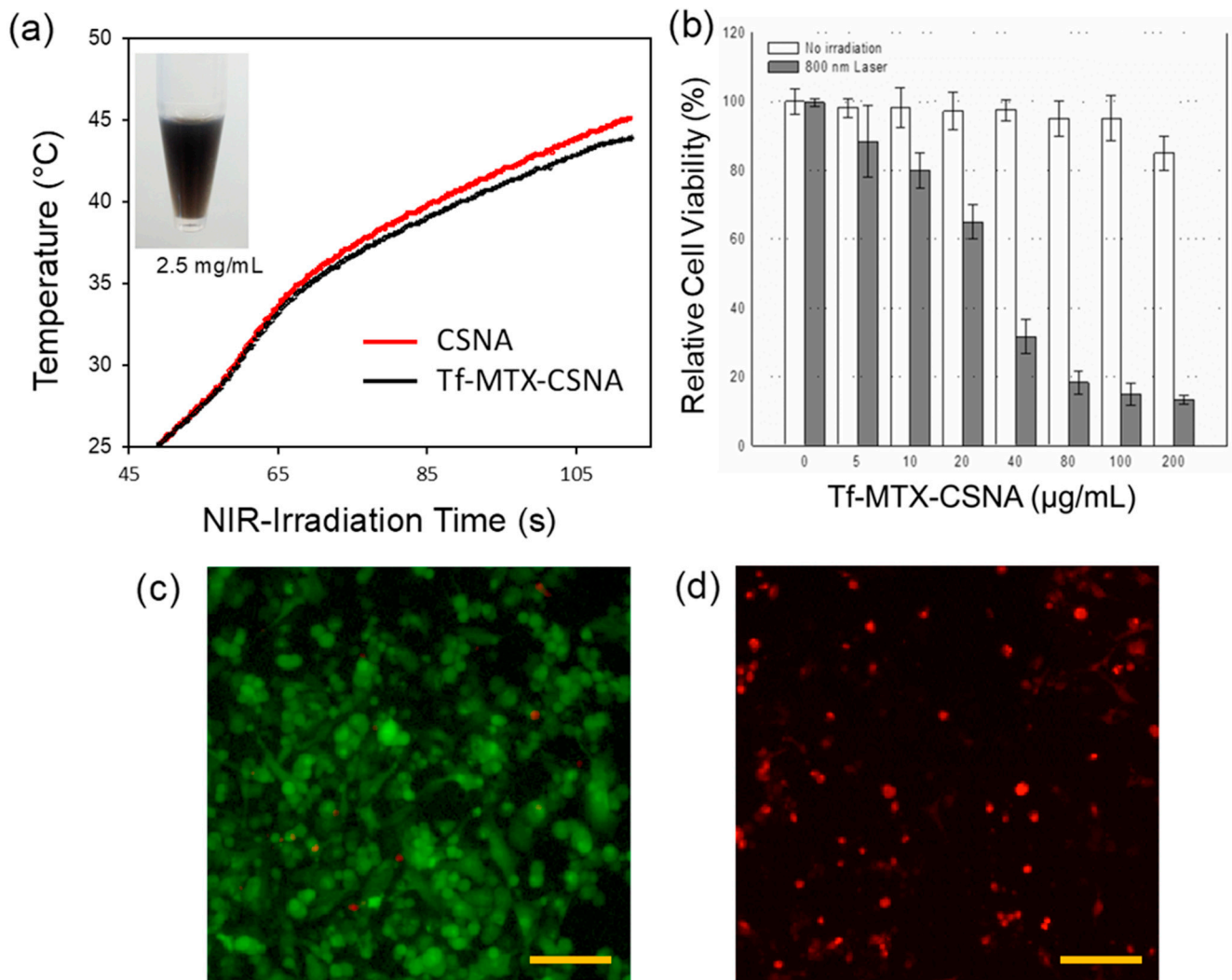


**Figure 7.** Photothermal activity of the CSNA samples. (a) Plot of the temperature increase by NIR-irradiation in the presence of CSNA and Tf-MTX-CSNA solution samples. In particular, the Tf-MTX-CSNAs showed similar magneto-thermal activity with bare CSNAs, confirming the outstanding magnetic stability after the conjugation processes. (b) XTT cytotoxicity assay as a function of the Tf-MTX-CSNA sample concentration. The fluorescence microscopic images of HeLa cells before (c) and after (d) the NIR exposure (scale bar: 100  $\mu\text{m}$ ).

As presented in Figure 8, the comparative AMF-induced magneto-thermal activity between the NPs all suspended in the same 0.1 M PBS buffer with a concentration of 2.5 mg/mL displayed the enhanced therapeutic effect of Tf-MTX-CSNAs over CSNAs. Subsequently, the samples were used as they are for the optical studies.

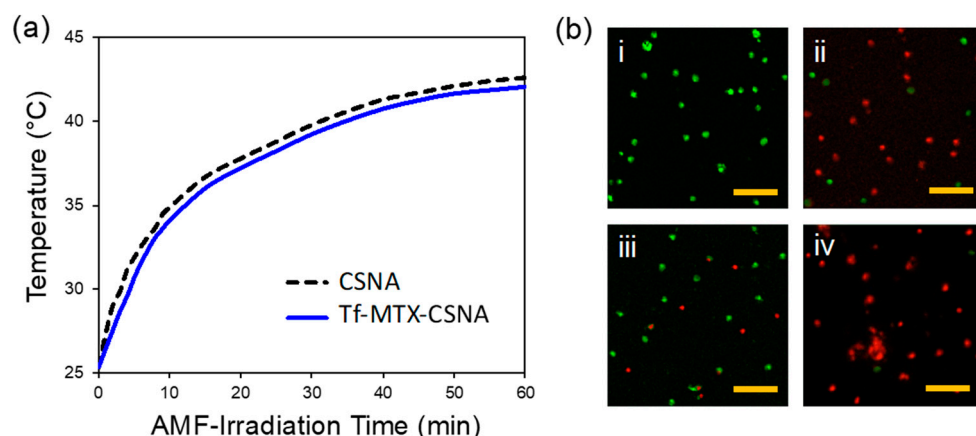


**Figure 8.** Magneto-thermal activity of the CSNA samples. (a) Plot of the temperature increase by AMF-irradiation. The Tf-MTX-CSNAs show similar magneto-thermal activity to bare CSNAs, confirming their outstanding magnetic stability after the conjugation processes. (b) Fluorescence images of HeLa cells in the presence of the CSNA (i,ii) and Tf-MTX-CSNA (iii,iv) samples, before (i,iii) and after (ii,iv) the AMF-treatments (scale bar: 100  $\mu$ m).

Unlike the synthesis method and functionality of the existing IONPs, the CSNAs showed a triggered-release behavior due to the magneto-thermal- and pH-responsive phase-changing property of the CSNA nanostructure under magneto-thermal -heating in an acidic medium (pH < 7), while exhibiting very slight release/leaking at pH > 7 by the magneto-thermal heating, as discussed in our previous result [8]. Conversely, in the MTX-CSNA and Tf-MTX-CSNA samples, no sustainable release of core Fe(salen) molecules was observed during either the photo-thermal- or magneto-thermal -activation for 60 min at pH 6, proving the robust stability of the coating interface during the heating process. Simultaneously, the tightly packed surface layer of MTX molecules by the biocompatible Tf proteins on the CSNA exterior was confirmed to shield it from possible undesirable side effects due to a leaking. There is not only a synergistic effect on the external hyperthermal effect, as a method for confirming and killing cancer without side effects; what can be inferred from the cell imaging results is that the Tf shell is attached to the Tf receptor on the surface of the cancer cell, in which the particles could be internalized through endocytosis. It would be possible to treat cancer by internalizing MTX loaded in the NPs into the cytoplasm and targeting nuclear or mitochondrial DNA to cause apoptosis/necrosis. Such a synergistically based anticancer system is similar to the concept presented in our previous study [23]. In order to confirm whether it can be a capable cancer-specific targeting at a tumor site, this should be explored in the future, followed by in vivo work.

In addition, in a similar research course using the metal salen and a conductive polymer, metal salen polymers exhibited many unique tunable properties, such as electro-catalytic activity, molecular sensing activity, electrochromic activity, and heterogeneous catalysis [24,25]. They have become promising candidates for a wide range of applications such as chemical sensors, renewable energy, and solar cells. However, to the best of our knowledge, this study is the first case of the application of metal salen nanocomposite particles with both magnetic and optical properties to biomedicine.

#### 4. Conclusions

We have synthesized a novel heterogeneous anticancer nanoarchitecture involved in organic and biological building blocks (organometals, block-co-polymers, proteins) by tailoring with CPy chemistry that led to the complex nano-drug hybrids, integrating the attractive material properties into multi-functionalities such as photo-thermal, magneto-thermal, and chemotherapeutic efficacy. Based on the in vitro assays and imaging, this resulted in a new proof-of-concept for dual-modal therapeutics that exploit optical and

magnetic modes of nano-hybrids, and also for chemotherapy which involves magnetic local targeting as an on-demand cancer treatment platform in a minimally invasive DDS fashion.

**Author Contributions:** Conceptualization, J.-H.K.; data curation and analysis, J.-H.K., M.U. and H.E.; project administration, J.-H.K.; funding acquisition, M.U. and Y.I.; writing—original draft, J.-H.K.; writing—review and editing, J.-H.K., M.U. and H.E. All authors have read and agreed to the published version of the manuscript.

**Funding:** This work was supported in part by the Japan Society for the Promotion of Science (IS), a Grant-in-Aid for JSPS Fellows (IS). This study was also supported in part by the Japan Society for the Promotion of Science (JSPS) KAKENHI Grant (25670131 to YI); The Ministry of Education, Culture, Sports, Science and Technology (MEXT) KAKENHI Grant (22136009 to YI); the New Energy and Industrial Technology Development Organization (NEDO; 60890021 to YI); the National Cerebral and Cardiovascular Center (NCVC; 22-2-3 to YI); the Japan Agency for Medical Research and Development (AMED; 66890005, 66890011, 66890001 and 66890023 to YI); and The Tokyo Biochemical Research Foundation (YI).

**Institutional Review Board Statement:** Not applicable.

**Informed Consent Statement:** Not applicable.

**Data Availability Statement:** Not applicable.

**Acknowledgments:** We are grateful to A. Nagasako, C. Oyamada, and M. Otake for their technical assistance in this study. Special thanks go to K. Yoshida (Japan Fine Ceramics Center) and T. Watanabe (FEI Gatan Inc., Japan) for the TEM tomography. The NIR laser system was supported by Okinawa Institute of Science and Technology.

**Conflicts of Interest:** The authors declare no conflict of interest.

## References

1. Lee, D.E.; Koo, H.; Sun, I.C.; Ryu, J.H.; Kim, K.; Kwon, I.C. Multifunctional nanoparticles for multimodal imaging and theragnosis. *Chem. Soc. Rev.* **2012**, *41*, 2656–2672. [[CrossRef](#)] [[PubMed](#)]
2. Lee, N.; Yoo, D.; Ling, D.; Cho, M.H.; Hyeon, T.; Cheon, J. Iron oxide based nanoparticles for multimodal imaging and magnetoresponsive Therapy. *Chem. Rev.* **2015**, *115*, 10637–10689. [[CrossRef](#)] [[PubMed](#)]
3. Stafford, S.; Serrano Garcia, R.; Gun'ko, Y.K. Multimodal Magnetic-plasmonic nanoparticles for biomedical applications. *Appl. Sci.* **2018**, *8*, 97. [[CrossRef](#)]
4. Kim, J.H.; Eguchi, H.; Umemura, M.; Ishikawa, Y. Hybrid metal complex nanocomposites for targeted cancer diagnosis and therapeutics. In *Materials for Biomedical Engineering: Inorganic Micro- and Nanostructures*; Elsevier: Amsterdam, The Netherlands, 2019; pp. 427–461.
5. Cianciaruso, C.; Pagani, A.; Martelli, C.; Bacigaluppi, M.; Squadrito, M.L.; Lo Dico, A.; De Palma, M.; Furlan, R.; Lucignani, G.; Falini, A.; et al. Cellular magnetic resonance with iron oxide nanoparticles: Long-term persistence of SPIO signal in the CNS after transplanted cell death. *Nanomedicine* **2014**, *9*, 1457–1474. [[CrossRef](#)] [[PubMed](#)]
6. Park, E.J.; Oh, S.Y.; Kim, Y.; Yoon, C.; Lee, B.S.; Kim, S.D.; Kim, J.S. Distribution and immunotoxicity by intravenous injection of iron nanoparticles in a murine model. *J. Appl. Toxicol.* **2016**, *36*, 414–423. [[CrossRef](#)]
7. Yang, L.; Kuang, H.; Zhang, W.; Aguilar, Z.P.; Xiong, Y.; Lai, W.; Xu, H.; Wei, H. Size dependent biodistribution and toxicokinetics of iron oxide magnetic nanoparticles in mice. *Nanoscale* **2015**, *7*, 625–636. [[CrossRef](#)]
8. Kim, J.-H.; Eguchi, H.; Umemura, M.; Sato, I.; Yamada, S.; Hoshino, Y.; Masuda, T.; Aoki, I.; Sakurai, K.; Yamamoto, M.; et al. Magnetic metal-complex-conducting copolymer core-shell nanoassemblies for a single-drug anticancer platform. *NPG Asia Mater.* **2017**, *9*, e367. [[CrossRef](#)]
9. Eguchi, H.; Umemura, M.; Kurotani, R.; Fukumura, H.; Sato, I.; Kim, J.-H.; Hoshino, Y.; Lee, J.; Amemiya, N.; Sato, M.; et al. A magnetic anti-cancer compound for magnet-guided delivery and magnetic resonance imaging. *Sci. Rep.* **2015**, *5*, 9194. [[CrossRef](#)]
10. Sato, I.; Umemura, M.; Mitsudo, K.; Fukumura, H.; Kim, J.-H.; Hoshino, Y.; Nakashima, H.; Kioi, M.; Nakakaji, R.; Sato, M.; et al. Simultaneous hyperthermia-chemotherapy with controlled drug delivery using single-drug nanoparticles. *Sci. Rep.* **2016**, *6*, 24629. [[CrossRef](#)]
11. Ohtake, M.; Umemura, M.; Sato, I.; Akimoto, T.; Oda, K.; Nagasako, A.; Kim, J.-H.; Fujita, T.; Yokoyama, U.; Nakayama, T.; et al. Hyperthermia and chemotherapy using Fe(Salen) nanoparticles might impact glioblastoma treatment. *Sci. Rep.* **2017**, *7*, 42783. [[CrossRef](#)]
12. Nakakaji, R.; Umemura, M.; Mitsudo, K.; Kim, J.-H.; Hoshino, Y.; Sato, I.; Masuda, T.; Yamamoto, M.; Kioi, M.; Koizumi, T.; et al. Treatment of oral cancer using magnetized paclitaxel. *Oncotarget* **2018**, *9*, 15591–15605. [[CrossRef](#)] [[PubMed](#)]

13. Umemura, M.; Kim, J.-H.; Aoyama, H.; Hoshino, Y.; Fukumura, H.; Nakakaji, R.; Sato, I.; Ohtake, M.; Akimoto, T.; Narikawa, M. The iron chelating agent, deferoxamine detoxifies Fe(Salen)-induced cytotoxicity. *J. Pharmacol. Sci.* **2017**, *134*, 203–210. [[CrossRef](#)] [[PubMed](#)]
14. Khan, Z.A.; Tripathi, R.; Mishra, B. Methotrexate: A detailed review on drug delivery and clinical aspects. *Expert. Opin. Drug Deliv.* **2012**, *9*, 151–169. [[CrossRef](#)] [[PubMed](#)]
15. Li, Y.; Lin, J.; Wu, H.; Jia, M.; Yuan, C.; Chang, Y.; Hou, Z.; Dai, L. Novel methotrexate prodrug-targeted drug delivery system based on PEG-lipid-PLA hybrid nanoparticles for enhanced anticancer efficacy and reduced toxicity of mitomycin C. *J. Mater. Chem. B* **2014**, *2*, 6534–6548. [[CrossRef](#)] [[PubMed](#)]
16. Gupta, J.; Bhargava, P.; Bahadur, D. Methotrexate conjugated magnetic nanoparticle for targeted drug delivery and thermal therapy. *J. Appl. Phys.* **2014**, *115*, 17B516. [[CrossRef](#)]
17. Alizadeh, N.; Shamaeli, E. Electrochemically controlled release of anticancer drug methotrexate using nanostructured polypyrrole modified with cetylpyridinium: Release kinetics Investigation. *Electrochim. Acta* **2014**, *130*, 488–496. [[CrossRef](#)]
18. Kim, J.-H.; Lu, T.M. Bio-inspired Janus composite nanoscroll for on-demand tumor targeting. *RSC Adv.* **2016**, *6*, 17179–17187. [[CrossRef](#)]
19. Ardani, H.K.; Imawan, C.; Handayani, W.; Djuhana, D.; Harmoko, A.; Fauzia, V. Enhancement of the stability of silver nanoparticles synthesized using aqueous extract of Diospyros discolor Willd leaves using polyvinyl alcohol. *IOP Conf. Ser. Mater. Sci. Eng.* **2017**, *188*, 012056. [[CrossRef](#)]
20. Yang, K.; Xu, H.; Cheng, L.; Sun, C.; Wang, J.; Liu, Z. In vitro and in vivo near-infrared photothermal therapy of cancer using polypyrrole organic nanoparticles. *Adv. Mater.* **2012**, *24*, 5586–5592. [[CrossRef](#)]
21. Osman, N.M. Polypyrrole as a thermoplasmonic. In Proceedings of the 2015 International Conference on Computing, Control, Networking, Electronics and Embedded Systems Engineering (ICCNEE), Khartoum, Sudan, 7–9 September 2015; pp. 475–478.
22. Wang, Y.; Meng, H.M.; Song, G.; Li, Z.; Zhang, X.B. Conjugated-polymer-based nanomaterials for photothermal therapy. *ACS Appl. Polym. Mater.* **2020**, *2*, 4258–4272. [[CrossRef](#)]
23. Kim, J.-H.; Eguchi, H.; Ishikawa, Y. Anticancer luminescent gold quantum clusters for in situ cancer-selective marking-imaging-targeting. *Nanoscale* **2017**, *9*, 9071–9082. [[CrossRef](#)] [[PubMed](#)]
24. Zhang, J.; Xu, L.; Wong, W.Y. Energy materials based on metal Schiff base complexes. *Coord. Chem. Rev.* **2018**, *355*, 180. [[CrossRef](#)]
25. Freire, C.; Nunes, M.; Pereira, C.; Fernandes, D.M.; Peixoto, A.F.; Rocha, M. Metallo(salen) complexes as versatile building blocks for the fabrication of molecular materials and devices with tuned properties. *Coord. Chem. Rev.* **2019**, *394*, 104. [[CrossRef](#)]